Possible quadrupolar nematic phase in the frustrated spin chain LiCuSbO4: An NMR investigation

Bosiočić, Marko; Bert, F.; Dutton, S. E.; Cava, R. J; Baker, P. J.; Požek, Miroslav; Mendels, P.

Source / Izvornik: **Physical Review B, 2017, 96**

Journal article, Published version
Rad u časopisu, Objavljena verzija rada (izdavačev PDF)

https://doi.org/10.1103/PhysRevB.96.224424

Permanent link / Trajna poveznica: https://urn.nsk.hr/urn:nbn:hr:217:479777

Possible quadrupolar nematic phase in the frustrated spin chain $LiCuSbO_4$: An NMR investigation

M. Bosiočić,[1,*] F. Bert,[2] S. E. Dutton,[3] R. J. Cava,[4] P. J. Baker,[5] M. Požek,[1] and P. Mendels[2]

[1]*Department of Physics, Faculty of Science, University of Zagreb, Bijenička 32, HR-10000 Zagreb, Croatia*

[2]*Laboratoire de Physique des Solides, CNRS, Université Paris-Sud, Université Paris-Saclay, 91405 Orsay Cedex, France*

[3]*Cavendish Laboratory, University of Cambridge, JJ Thomson Avenue, Cambridge CB3 0HE, United Kingdom*

[4]*Department of Chemistry, Princeton University, Princeton, New Jersey 08544, USA*

[5]*ISIS Facility, STFC Rutherford Appleton Laboratory, Didcot OX11 0QX, United Kingdom*

(Received 15 October 2017; revised manuscript received 5 December 2017; published 20 December 2017)

The frustrated one-dimensional quantum magnet $LiCuSbO_4$ is a rare realization of the J_1-J_2 spin chain model with an easily accessible saturation field, formerly estimated at 12 T. Exotic multipolar nematic phases were theoretically predicted in such compounds just below the saturation field, but without unambiguous experimental observation so far. In this paper we present extensive experimental research on the compound in a wide temperature (30 mK to 300 K) and field (0–13.3 T) range by muon spin rotation (μSR), ^{7}Li nuclear magnetic resonance (NMR), and magnetic susceptibility (SQUID). μSR experiments in zero magnetic field demonstrate the absence of long-range 3D ordering down to 30 mK. Together with former heat capacity data [Dutton *et al.*, Phys. Rev. Lett. **108**, 187206 (2012)], magnetic susceptibility measurements suggest a short-range-correlated vector chiral phase in the field range 0–4 T. At the intermediate-field values (5–12 T), the system enters a 3D-ordered spin density wave phase with 0.75 μ_B per copper site at lowest temperatures (125 mK), estimated by NMR. At still higher field, the magnetization is found to be saturated above 13 T where the spin lattice T_1^{-1} relaxation reveals a spin gap estimated at 3.2(2) K. We narrow down the possibility of observing a multipolar nematic phase to the range 12.5–13 T.

DOI: 10.1103/PhysRevB.96.224424

I. INTRODUCTION

The simple Heisenberg Hamiltonian describing an ideal one-dimensional (1D) spin $S = 1/2$ system with only nearest-neighbor (NN) antiferromagnetic interactions was solved by Bethe in 1931. This remains until today one of the rare analytical solutions of such a Heisenberg Hamiltonian. Real materials also require the introduction of additional interactions, e.g., the next-nearest-neighbor (NNN) interaction, Dzyaloshinskii-Moriya (DM) interaction, effects of anisotropy, etc. Analytical solutions, especially in the quantum case, often do not exist, but the development of numerical methods has unveiled theoretical phase diagrams predicting the existence of novel exotic phases whose properties are not yet completely understood, making 1D quantum spin systems a rich research topic in contemporary condensed matter physics.

In this vein, special attention was recently given to phases which do not break time-reversal symmetry, i.e., $\langle S\rangle = 0$, but are governed by spin tensor parameters hence named higher-rank multipolar-driven phase transitions, the quadrupolar being the simplest. Such a spin-nematic phase breaks O(3) spin symmetry but does not possess any magnetic moment [1]. It was first proposed in systems with on-site spin $S \geqslant 1$ [2], and later a similar order was predicted in spin $S = 1/2$ systems based on bond order parameters [3]. This could occur in frustrated Heisenberg spin $S = 1/2$ chains under an applied field h, with a specific scheme of ferromagnetic (FM) nearest-neighbor (J_1) and antiferromagnetic (AFM) next-nearest-neighbor interactions (J_2) [4–8]:

$$H = J_1 \sum_i \mathbf{S}_i \mathbf{S}_{i+1} + J_2 \sum_i \mathbf{S}_i \mathbf{S}_{i+2} - h \sum_i S_i^z. \qquad (1)$$

For systems with a J_1/J_2 ratio in the range $[-2.7,0]$ three successive field-induced phases are predicted: a vector chiral (VC) phase in the low-field region, a spin density wave (SDW_2) phase of 2 bound magnons in intermediate fields, and a quadrupolar nematic (QN) phase above $\approx$70% of the saturation magnetization [8].

The direct experimental observation of a QN phase is demanding, since most local techniques are not sensitive to the dominant four-point correlation function $\langle S_0^+ S_1^+ S_l^- S_{l+1}^-\rangle$, where $0, 1, l$, and $l+1$ denote the positions of spins in a chain. Sato *et al.* [9] suggested that NMR could indirectly probe the existence of the QN phase through the temperature dependence of the spin-lattice relaxation rates $1/T_1$.

An ideal compound should have negligible interchain interactions to avoid 3D ordering and small intrachain interaction parameters J_1 and J_2 in order to reach the saturation of magnetization with H-T parameters available in laboratories. Among J_1-J_2 Heisenberg compounds, $LiCu_2O_2$ [10], Li_2CuO_2 [11], $Cs_2Cu_2Mo_3O_{12}$ [12], $Rb_2Cu_2Mo_3O_{12}$ [13], $LiCuVO_4$ [14], $PbCuSO_4(OH)_2$ [15], and $LiCuSbO_4$, the three latter have been suggested as possible candidates to stabilize a QN phase in appropriate field conditions. A recent "tour de force" NMR study on $LiCuVO_4$ [16] in pulsed high magnetic field up to 56 T pinpointed a microscopic signature of the QN phase, but no T_1 measurements could be performed. For linarite $PbCuSO_4(OH)_2$, the stabilization of spin multipolar phases is now questioned by a recent neutron-scattering experiment [17]. Finally, the recently discovered $LiCuSbO_4$ compound [18], with the estimated coupling constants $J_1 = -75$ K and $J_2 = 34$ K and rather low saturation field $\mu_0 H_S \approx 12$–13 T, seems to be a very promising candidate for the realization of a QN phase: (i) No 3D ordering in zero field was observed down to $T = 100$ mK which indicates that interchain couplings are negligible. (ii) Neutron measurements together with

*marko.bosiocic@gmail.com

susceptibility data show that short-range correlations emerge below 9K, at temperatures depending on the magnitude of the applied magnetic field. (iii) An anomaly in the specific heat is detected for $T \sim 0.7$ K which is enhanced on the application of a field and disappears for $\mu_0 H \geqslant 13$ T. One possible origin of this peak was suggested to be a multipolar transition in the vicinity of the saturation field.

In this paper we present an *H-T* study of $LiCuSbO_4$ combining susceptibility, μSR, and NMR measurements in the sub-Kelvin range, up to 13.3 T. As compared to a recent NMR study published in the course of our work [19], ours is performed on an oriented powder sample and at temperatures down to 30 mK. Through the line shapes, we can monitor the various ground states under an applied field and we accurately determine the saturation field from the variation of the local magnetization determined through the line shift. We sketch a phase diagram combining our systematic analysis of NMR spectra, T_1 relaxation times, and μSR data, together with bulk magnetization measurements and former data from Ref. [18]. Our analysis shows that $LiCuSbO_4$ is indeed a very good candidate for the realization of a QN phase in the field range between 12.5 and 13 T. Our results partly differ from Ref. [19] and are discussed with respect to that work.

The paper is structured as follows: In Sec. II, we give details about the sample preparation, structure, and procedure used to orient the NMR sample. In Sec. III we present our μSR results in zero field down to 30 mK. Section IV gives our SQUID experiment results from low field to 7 T, down to 300 mK. The NMR spectral analysis is presented in Sec. V, where we also discuss the saturation field value which is crucial for the determination of the field range where a QN phase can be expected. Field- and temperature-dependent NMR spin lattice relaxation T_1^{-1} measurements are presented in Sec. VI. In the discussion we compare the compound with other possible 1D candidates described by the J_1-J_2 Hamiltonian and finally build the *H-T* phase diagram from all available experimental data on $LiCuSbO_4$.

II. CRYSTAL STRUCTURE AND SAMPLE PREPARATION

$LiCuSbO_4$ crystallizes in the space group $Cmc2_1$ with tetragonal unit cell ($a = 5.74260$ Å, $b = 10{,}86925$ Å, $c = 9.73048$ Å). The copper ions Cu^{2+} carry $S = 1/2$ spins. The structure is shown in Fig. 1 [20]. The basic building blocks are edge-sharing CuO_6 octahedra which form chains along the *a* axis. The Cu-O bonds perpendicular to the *a* axis are significantly elongated, defining local *z* axes for each chain as marked in Fig. 1. The *z* axes of the CuO_6 octahedra in adjacent chains are not parallel, but canted 34° in opposite directions with respect to the *b* axis. The unit cell contains two crystallographic positions of lithium, Li(1) and Li(2), slightly distributed along the *b* axis and *a* axis, respectively. Crystallographically, this is modeled as two close sites with 50% occupancy [18]. Polycrystalline samples were synthesized as explained in Ref. [18]. For the magnetization and NMR measurements, the polycrystalline powder was ground and mixed with an epoxy glue and during the hardening, the sample was rotated around an axis perpendicular to a magnetic field ≈7 T for 24 h. This procedure ensures that the hard magnetization axis of the sample aligns with the rotation axis. The orientation of the powder sample was checked by NMR as described in Appendix A. Further x-ray diffraction refinements on the oriented sample have shown that the rotation axis is perpendicular to the *a* axis; i.e., the hard axis lies in the *bc* plane. In NMR and magnetization measurements the magnetic field was applied along the hard axis, perpendicular to the direction of the chains (*a* axis).

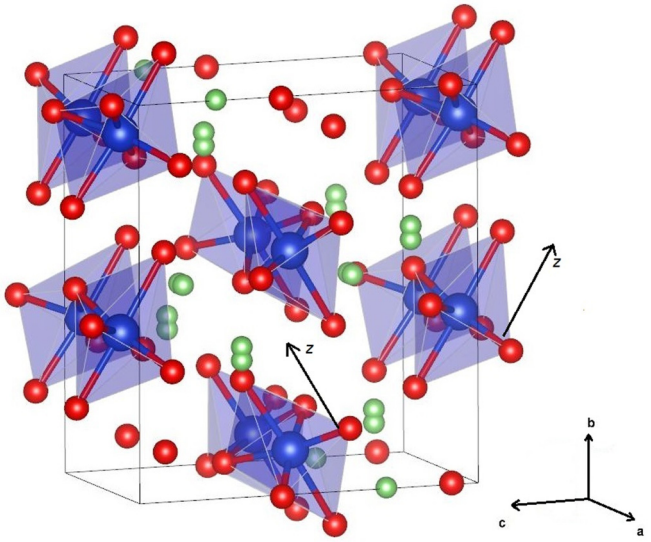

FIG. 1. Crystal structure of $LiCuSbO_4$. Unpaired spins are localized on Cu^{2+} ions (blue) centered in CuO_6 octahedra. Edge-sharing octahedra form spin chains parallel to the *a* axis. The local *z* axes of two adjacent spin chains are canted by 34° in opposite directions with respect to the *b* axis. Distribution of Li(1) (green) is supposed to be in the direction of the *b* axis, while Li(2) in the direction of the *a* axis. Oxygen atoms are labeled in red color. Antimony ions are omitted for clarity.

III. μSR MEASUREMENTS

In previous heat capacity measurements [18], no magnetic transition was observed down to 100 mK. However signatures of spin-glass-like states or subtle spin freezing involving only part of the spin degrees of freedom are often elusive in such measurements. In order to confirm the nature of the zero-field ground state on a firmer ground, we performed μSR measurements which are extremely sensitive to even tiny internal fields [21]. The measurements were performed at the ISIS pulsed muon source facility (UK) on the MUSR spectrometer. We used a powder sample ≈1 g from the same batch as for the NMR measurements. The loose powder sample was spread on a silver holder plate and covered with drops of diluted GE varnish to ensure a good thermal contact. A helium-bath cryostat with a dilution refrigerator insert was used for temperature control in the range 0.03 K to 10 K.

Muon decay asymmetries recorded at the highest and base temperatures of the experiment are shown in Fig. 2. At high temperature the zero-field relaxation is dominated by the rather strong Cu and Li nuclear moments which are disordered and static on the muon time scale. The initial Gaussian shape is characteristic of the static Kubo-Toyabe relaxation $G(t, \Delta, 0)$

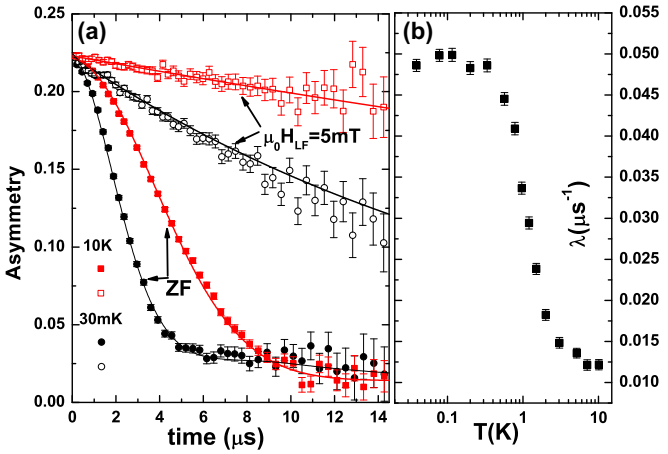

FIG. 2. (a) Asymmetries of the muon decay in zero field (solid symbols) and with a small 5 mT longitudinal field (open symbols) at 30 mK and 10 K. Lines are fits to the data (see main text). (b) Temperature dependence of the muon relaxation rate extracted from exponential fits of the muon decay asymmetry measured with a 5 mT applied longitudinal field.

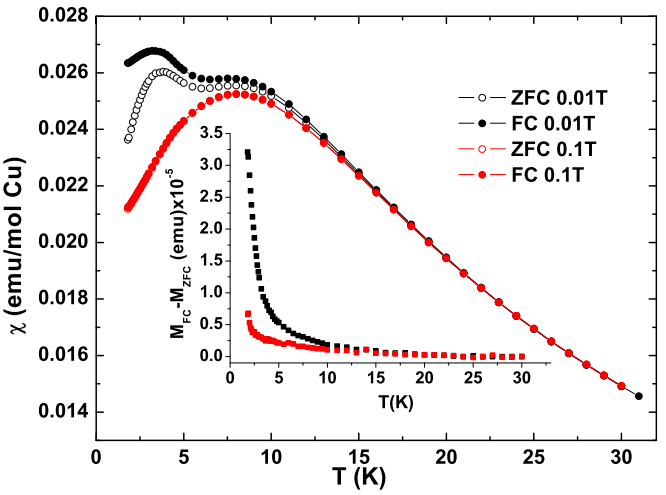

FIG. 3. Low-field susceptibility measurement on an unoriented powder sample. In the magnetic field of 0.01 T, FC and ZFC susceptibility start to differ at 15 K. Upon increasing magnetic field this difference vanishes. Inset show differences between between FC and ZFC magnetization curves in a field of 0.01 T (black) and 0.1 T (red).

expected for frozen random fields with a distribution width Δ [22,23]. However, the "1/3rd" recovery at long times of the Kubo-Toyabe function is not observed here, likely because of numerous muon stopping sites and nuclear moments sizes. In addition to nuclear magnetism, the fast-fluctuating electronic moments contribute to a weak exponential relaxation which can be isolated by applying a small longitudinal field of 5 mT to decouple the nuclear static relaxation as shown in Fig. 2. The 10 K asymmetries were thus fitted to the model

$$a(t) = a_0 P(t) \exp(-\lambda t) + a_b \qquad (2)$$

with $P(t) = \exp(-\sigma^2 t^2)$ in zero field and $P(t) = 1$ for a 5 mT applied field. The T-independent parameters $a_0 = 0.220(5)$ and $a_b = 0.014(5)$ stand for the initial muon decay asymmetry and the fraction of muons stopping in the silver sample holder. From the Gaussian decay $\sigma = 0.18(1)\ \mu s^{-1}$ and the muon gyromagnetic ratio $\gamma_\mu = 2\pi \times 135.54$ MHz/T, we estimate the frozen field distribution width $\Delta \approx \sigma/\gamma_\mu = 0.21(1)$ mT consistent with nuclear magnetism.

Upon cooling the relaxation increases gradually down to 0.03 K where the zero-field asymmetry shows a steeper Gaussian decay and crosses the 10 K one around 9 μs. This crossing cannot be accounted for by a mere change in the dynamical relaxation [the exponential decay in Eq. (2)]. It implies a nonmonotonic variation of $P(t)$, hence the development of frozen internal fields at base temperature, besides the nuclear ones which are temperature independent. However and most remarkably, these static internal fields are surprisingly small since they produce a relaxation hardly faster than the 10 K one due to nuclear fields. To quantify these model-free observations, we fitted the 0.03 K data to Eq. (2) (see black solid lines in Fig. 2). For the zero-field asymmetry we used $P(t) = G(t, \Delta, \nu)$, the dynamical Kubo-Toyabe relaxation which accounts for essentially static internal fields with $\Delta = 0.42(2)$ mT, slowly fluctuating at the rate $\nu = 0.26(1)$ MHz $\ll \gamma_\mu \Delta$. For comparison, one can estimate the level of spin ordering as follows. Making the usual assumption that muons stop close to negatively charged O^{2-} ions, $\approx$2 Å away from the Cu^{2+} sites, in the hypothetical case of full ordering with 1 μ_B per Cu ion, one would expect dipolar local field $\mu_0 \mu_B/(4\pi r^3) \approx 0.12$ T at the muon sites. The observed local fields are three orders of magnitude lower and one can discard standard magnetic phases with on-site frozen moments as the zero-field ground state. It is possible that the marginal spin freezing reflects the existence of short-range correlations as suggested in Ref. [18].

Since the static internal fields remain weak in the whole T range, the dynamical relaxation channel can be probed in isolation down to 0.03 K by applying the same small 5 mT longitudinal field as at 10 K. The relaxation remains exponential at all T. The temperature dependence of the λ parameter of Eq. (2) is shown in Fig. 2(b). The increase of λ signals a moderate slowing down of the spin dynamics as if the system were approaching a transition around 1 K. However, instead of diverging and decreasing below 1 K, λ levels off showing the persistence of slow fluctuations in the ground state. The absence of a peak in $\lambda(T)$ is further evidence for the absence of 3D ordering or even standard spin-glass freezing in $LiCuSbO_4$ down to 0.03 K.

IV. LOW-TEMPERATURE MAGNETIC SUSCEPTIBILITY

The magnetization of both an oriented and an unoriented powder sample, prepared as described in Sec. II, were measured versus temperature in various magnetic fields in a commercial MPMS-7 Quantum Design SQUID magnetometer equipped with a ^{3}He insert for sub-Kelvin measurements. In the lowest investigated field of 0.01 T, a small difference between the field-cooled and zero-field-cooled susceptibilities is observed below about 15 K (see Fig. 3). This irreversibility is very weak in 0.1 T and disappears upon applying higher fields. The occurrence of some level of spin freezing in low field is consistent with the μSR data.

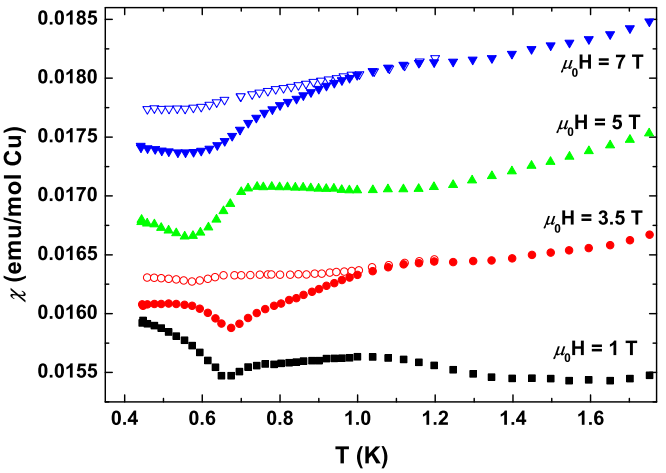

FIG. 4. Low-temperature magnetic susceptibility of the oriented powder $LiCuSbO_4$ with magnetic field parallel to the average hard axis (full symbols). The curves are shifted vertically for clarity. Empty symbols: For comparison, susceptibility of the unoriented powder sample at 3.5 and 7 T.

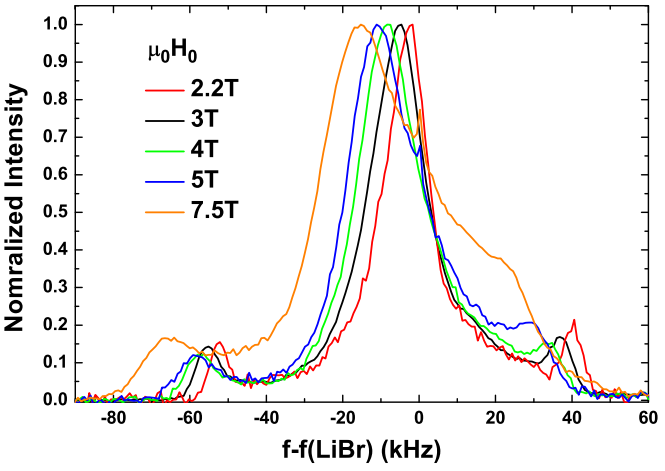

FIG. 5. Room temperature ^{7}Li spectra in various magnetic fields (up to 7.5 T). At low fields one can clearly distinguish the quadrupolar satellites of the Li site with the highest quadrupolar coupling.

We have further measured the low-temperature magnetic susceptibility of an oriented powder sample in four characteristic fields (Fig. 4) applied along the hard axis, perpendicular to the direction of the chains. All the measured susceptibility curves show some feature at $T = 0.7$ K, indicating the existence of a phase boundary. In the lower fields (1 T and 3.5 T), the transition is defined by a sharp minimum, while at higher fields (5 T and 7 T) an increase of χ occurs at the same temperature. These different features suggest that the low-temperature phases are distinct; i.e., there exists a phase boundary, when the field is increased at constant temperature, between 3.5 T and 5 T. Similar small changes in the signatures of the transitions were observed in single crystals of linarite $PbCuSO_4(OH)_2$ and used to draw its complex magnetic phase diagram [15]. For comparison, the transitions in $LiCuSbO_4$ are even weaker and hardly detectable in an unoriented powder sample (empty symbols in Fig. 4), and could be easily overlooked.

V. NMR SPECTRA AND DETERMINATION OF THE SATURATION FIELD

NMR measurements were performed on ^{7}Li nuclear spin $I = 3/2$ ($\gamma/2\pi = 16.54607$ MHz/T). The spectra were obtained using a solid echo sequence $\pi/2$-τ-$\pi/2$, with a pulse length between 1.5 μs and 3 μs when the helium flow cryostat was used and 10 μs in the dilution fridge environment. A solution of LiBr in deionized water was used to determine the NMR reference frequency ν_0.

Spectra at room temperature in magnetic fields up to 7.5 T are shown in Fig. 5. At low fields, below 5 T, the central lines from the two crystallographic lithium sites Li(1) and Li(2) overlap and a pair of quadrupolar satellites with $\nu_Q = 47(1)$ kHz is clearly resolved. Since the pulse length was optimized for the central transition, the quadrupolar satellites are less excited, and the theoretical ratio 3:4:3 for the central line and satellites intensities is not obeyed. As the field is increased, these central lines of the two Li sites start to differ due to different hyperfine coupling constants and the central line coming from the less-coupled one starts to overlap with the right quadrupolar satellite of the other.

The evolution of the spectral shape at 7.5 T with decreasing temperature can be followed in Fig. 6. The spectral line shifts to lower frequencies and simultaneously broadens magnetically. Eventually, the quadrupolar satellites cannot be resolved anymore below about 80 K. The broad NMR spectra are obtained by combining partial spectra measured at periodically spaced irradiation frequencies.

To estimate the strength of the coupling between the ^{7}Li nuclei and the Cu electron spins, we compare the spectral shift $K = (\nu - \nu_0)/\nu_0$ to the macroscopic magnetic susceptibility χ_{macro} measured at similar fields, respectively 7.5 T and 8 T (see Fig. 7), using the general relation

$$K = A_{\text{hf}}\chi_{\text{macro}} + K_0, \tag{3}$$

where K_0 is the temperature-independent orbital shift, and A_{hf} is the hyperfine coupling, assumed to be isotropic. Although there are two Li lines corresponding to the two Li sites, with different hyperfine coupling constants, we could only track reliably, over the whole temperature range, the shift of the maximum of the spectra corresponding to the most coupled Li site (see below Fig. 8). As shown in the Jaccarino plot in the inset of Fig. 7, Eq. (3) is satisfied on a large T range down to about 9 K which yields the hyperfine coupling constant $A_{\text{hf}} = -0.57(2)$ kOe/μ_B and $K_0 = 0(6)$ ppm.

Below 9 K, the NMR shift and the macroscopic susceptibility start to differ slightly. This difference may be due to the fact that the NMR shift was measured on an oriented powder sample, while the SQUID data were measured on an unoriented one. Furthermore, even a tiny amount of impurities with Curie-like contributions can alter the macroscopic susceptibility at low temperature while the NMR shift at peak position remains unaffected. The smallness of the difference between the two measurements, both showing clearly a maximum, supports the high quality of the sample and the claim for an upper limit of

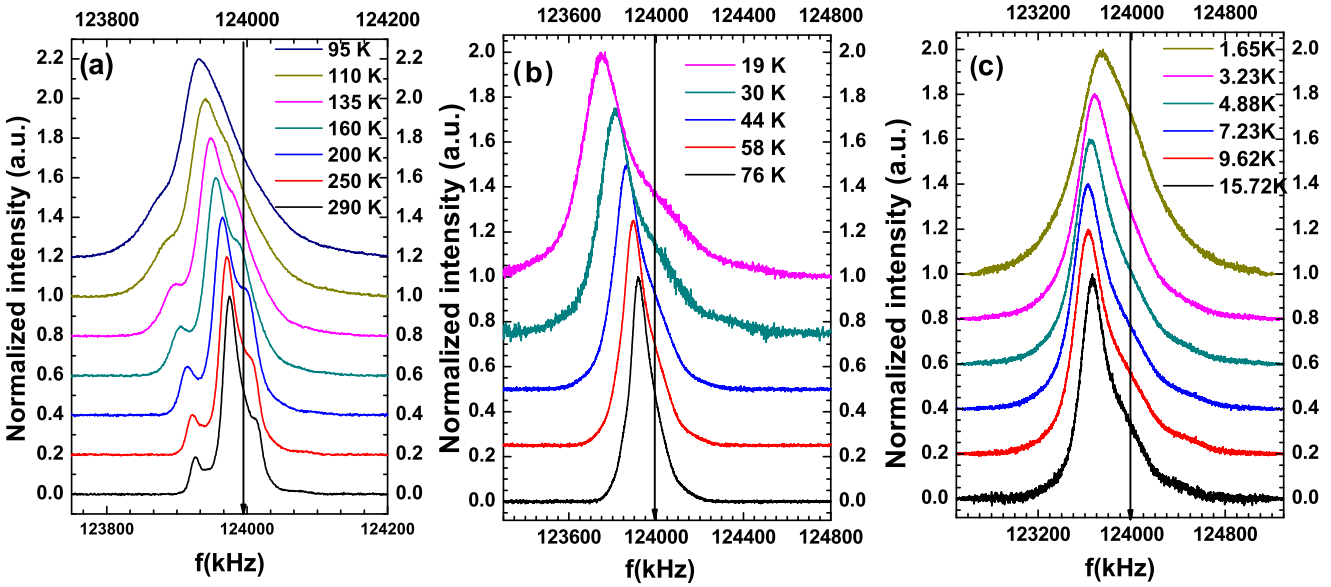

FIG. 6. Spectra at $\mu_0 H = 7.5$ T for different temperatures. The vertical lines denote the reference frequency ν_0.

the impurity concentration, such as Li/Cu or Sb/Cu intersite mixing, of 1% [18].

When the magnetic moment increases (by applying a higher magnetic field or by lowering the temperature), the typical spectral shape resembles the one shown in Fig. 8 ($\mu_0 H_0 = 12$ T at 1.55 K). The spectrum is well simulated by a Lorentzian line for the strongly coupled site and a Gaussian line for the weakly coupled one. The ratio of their intensities is 55:45 in favor of the Lorentzian line. The contribution of the weakly coupled site to the amplitude of the main peak is ≈28%.

At lower temperatures, below 1 K, the spectral shape considerably changes and becomes strongly field dependent as shown in Fig. 9. The vertical line in that figure denotes the maximum shift of 0.057 T using the hyperfine constant and assuming a full 1 μ_B moment per Cu site. The spectral widths at 0.125 K are substantially larger than the one at 1.55 K in the corresponding fields. These broad spectra are obtained at fixed irradiation frequencies ν_0 by field sweeps around the reference field $\mu_0 H_0 = 2\pi\nu/\gamma$. The squarish shape of the 5.2 T spectrum is characteristic of the powder average in a magnetically ordered system where all nuclei experience the same magnitude of the hyperfine field. From the spectral width one can estimate the amplitude of the on-site Cu moment to be 0.75 μ_B. The narrower component on top of the squarish one can likely be assigned to the less-coupled site. In stronger applied fields, the spectra become narrower (inset in Fig. 9) and shifted towards higher fields. This is the expected consequence of the increasing polarization of the system towards saturation when all the spins point in the same direction along the applied field. The spectra at 13 T and 13.3 T overlap indicating that the

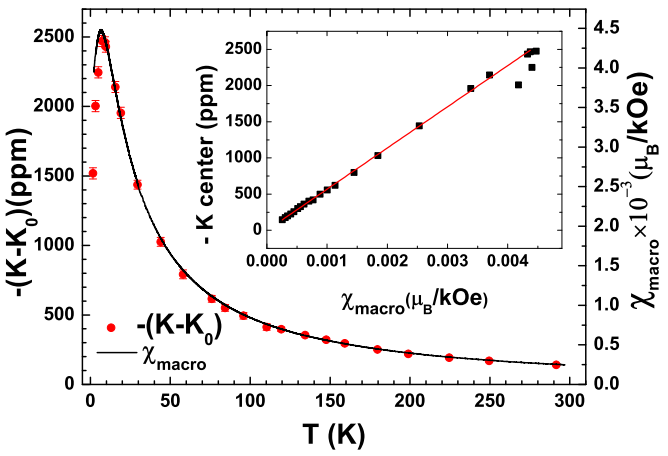

FIG. 7. Temperature dependence of the NMR shift (red circles) and macroscopic SQUID susceptibility (line). Inset: The Jaccarino plot shows the dependence of the NMR shift on the macroscopic magnetic susceptibility measured at 8 T.

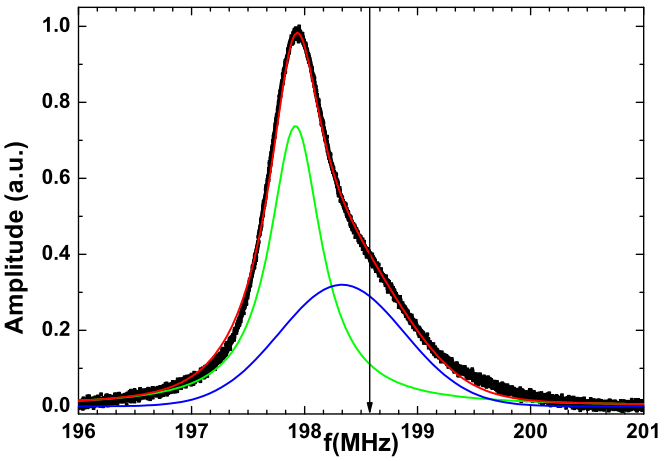

FIG. 8. Spectrum recorded at $T = 1.55$ K in magnetic field $\mu_0 H_0 = 12$ T (black). The red line is a simulation composed of a Lorentzian (green) and Gaussian (blue) line. Ratio of integrated intensities is 55:45 in favor of the Lorentzian line. The contribution of the Gaussian line at the main peak position is ≈28%. The vertical line shows the shift reference.

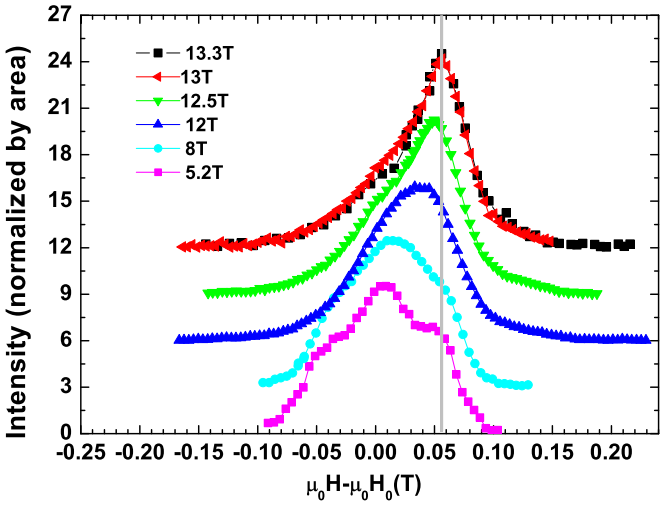

FIG. 9. Spectra obtained by field sweeps at different frequencies ($\nu = \gamma\mu_0 H_0$) at $T = 0.125$ K. The vertical line represents the maximum hyperfine field of 0.057 T corresponding to 1 μ_B per Cu site. This value was obtained independently from the Jaccarino plot; hence, the peak positions of the spectra in the saturation regime are right where we expect them to be. At 5.2 T and 8 T spectra are squarish in shape indicating spin freezing. As the field increases, the system polarizes and the spectra narrow. The inset shows the full width at half maximum (FWHM) of the spectra in the main panel. The gray line is a guide to the eyes.

system is fully polarized above 13 T. The shift value for the spectra at 13 T and 13.3 T matches perfectly the maximum shift value calculated independently from the determination of the hyperfine constant at high temperatures (the analysis of Jaccarino plot from Fig. 7). The maximum shift value is denoted by a vertical line in in Fig. 9.

The saturation field value of $LiCuSbO_4$ was formerly estimated from bulk magnetization data at 2 K on a powder sample (full red line in Fig. 10) [18]. The full saturation was not reached for the highest 16 T available field although an

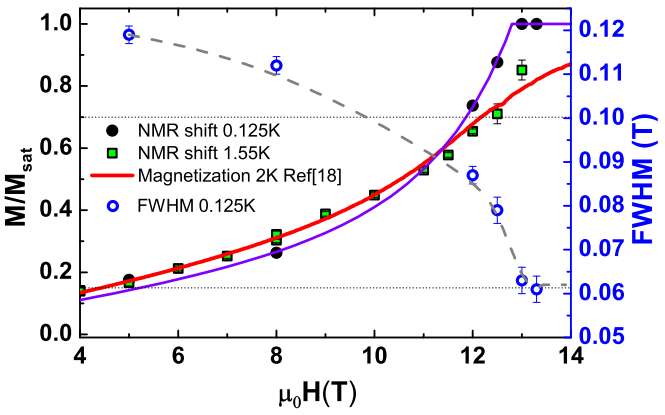

FIG. 10. Field dependence of the NMR peak position at $T = 0.125$ K (black circles) and $T = 1.55$ K (green squares) compared to the bulk magnetization at 2 K from Ref. [18] (red line). The purple line is a guide to the eyes for the $T = 0.125$ K NMR data. Right axis: FWHM of the spectra at 0.125 K (blue empty circles). The dashed line is a guide to the eyes.

inflection occurs roughly between 12 and 13 T. The magnetization curve could be tentatively reproduced by introducing exchange anisotropy but finite-temperature effects, powder averaging, and possible impurity contributions preclude a precise determination of the saturation field which is extremely important in the search for the QN phase.

An alternative way to estimate the saturation field is the measurement of the local magnetization at the ^{7}Li site through the position of the NMR line shift (Fig. 9), with the advantage of using an oriented powder sample. The field dependence of the NMR shift at $T = 0.125$ K is shown by full circles in Fig. 10. It is clear that the magnetization is still not saturated at 12.5 T, but that it is saturated at 13 T. Compared to the bulk magnetization data taken at $T = 2$ K on unoriented powder [19], the increase of the NMR shift is much steeper around 12 T.

To check the effect of temperature, we have also measured NMR shifts at $T = 1.55$ K (squares). The data correspond better to the bulk magnetization at 2 K, despite the sample orientation for the NMR measurements. In conclusion, we estimate the saturation field of $LiCuSbO_4$ to be larger than 12.5 T and slightly below 13 T. The sharp transition to saturation is observed only at $T = 0.125$ K, while the increased temperature and/or the lack of orientation smears out this transition. Hence, we emphasize the advantage for the determination of the saturation field to investigate the local magnetization at very low temperatures, preferably on oriented powder.

VI. RELAXATION MEASUREMENTS

For the measurements of the spin-lattice relaxation times T_1, a saturation-recovery pulse sequence was used. The first saturation pulse (4–5 μs) rotates the nuclear magnetization in the xy plane. After a waiting time τ_1, the longitudinal magnetization recovered along z, the direction of the applied field, is detected with a standard solid echo sequence with 3 μs $\pi/2$ pulses. Typical recovery curves are shown in Fig. 11. For applied field lower or equal to 12 T, at all temperatures, the recovery curve at the central peak position of the spectrum could be fitted to a single exponential giving a straightforward determination of T_1 [Fig. 11(a), red circles]. Above 12 T and below 5 K, the shape of the recovery changes and cannot be reproduced by a single exponential function [Figs. 11(a) and 11(c)]. This is certainly related to the occurrence of significantly different relaxation times for various spectral segments [Fig. 11(b)]; namely, the left part of the spectrum (strongly coupled line) is relaxing slower than the right one. To take into account these different contributions of the two Li sites at the main peak position (see Fig. 8), we used a function of the general form

$$1 - \frac{M(\tau_1)}{M_\infty} = ae^{-(\tau_1/T_1)^\beta} + (1-a)f(\tau_1), \qquad (4)$$

where M_∞ is the magnetization at equilibrium, a, the weight of the best coupled site, could be fixed to 0.72 in line with the analysis of the spectral shape in Fig. 8, and $f(t)$ is the residual relaxation associated with the least-shifted site which could be determined independently by measurements on the right side of the spectrum (see Appendix B). The T-dependent stretched

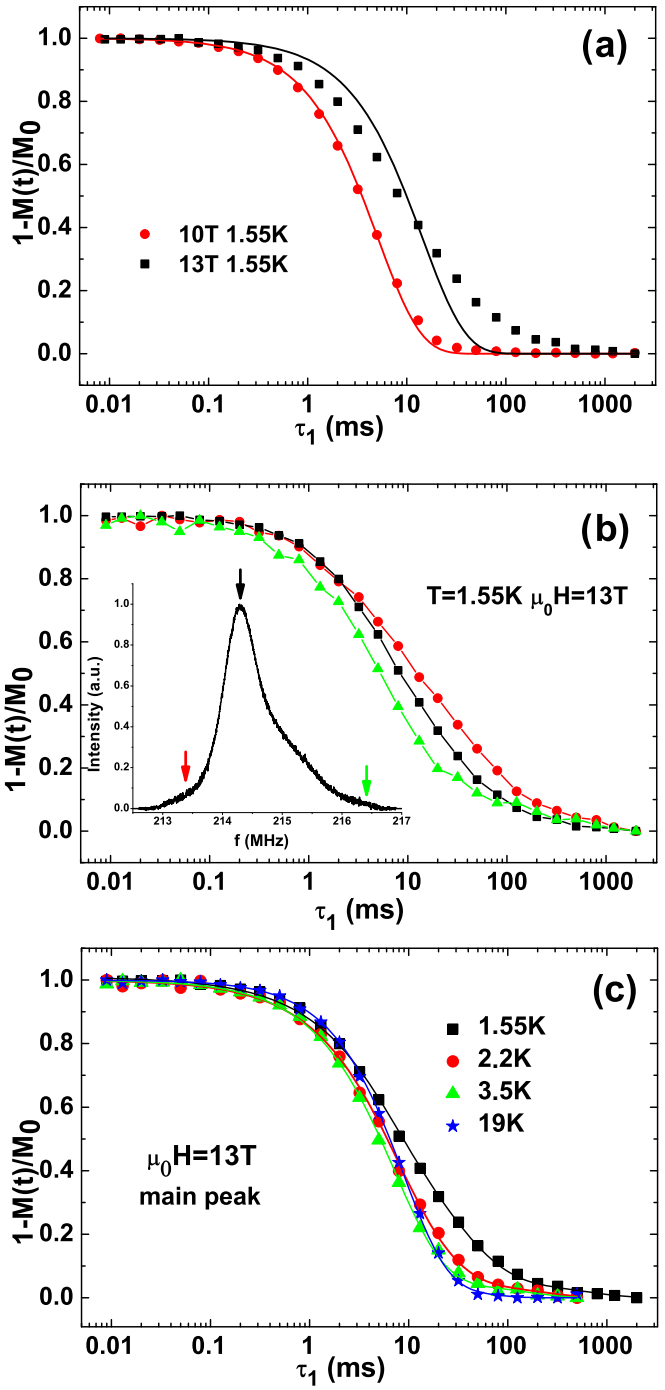

FIG. 11. (a) Spin-lattice relaxation (central peak) measured at $T = 1.55$ K at $\mu_0 H = 10$ T (red circles) and at $\mu_0 H = 13$ T (black squares). The lines are single-exponential fits. (b) Relaxation of the magnetization at different parts of spectra at the temperature $T = 1.55$ K. Arrows on the spectra correspond to frequencies where relaxation was measured. Lines are guide for the eyes. (c) Relaxation curves at the main peak at various temperatures. Full lines are obtained by the fit to Eq. (4).

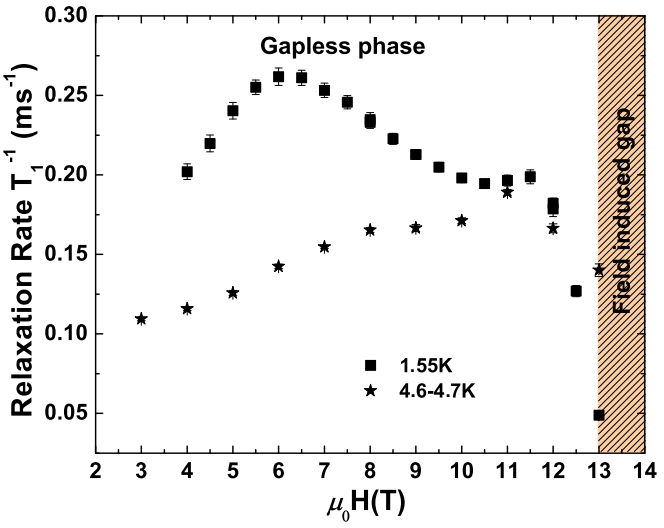

FIG. 12. Field dependence of the relaxation rate at $T = 1.55$ K and $T = 4.6$ K. The peak around 6 T at $T = 1.55$ K may be a reminiscence at finite T of the crossover between the VC and SDW_2 phases. T_1 drastically changes above $\mu_0 H \approx 12$ T, and above $\mu_0 H = 13$ T the system is in the field-induced-gap phase. Between 12 T and 13 T it is plausible to search for the possible existence of a QN phase.

exponent $\beta < 1$ accounts for an increasing distribution of the T_1 values at low $T < 5$ K [see inset of Fig. 13(b)]. Such a distribution may be due to some local excitations which can be an intrinsic property of chains or due to impurities (switching Cu with Li or Sb [18]) or defects (vacancies and chain edges). The upper limit for the impurity concentration is 1% but they can significantly perturb a dozen neighboring spins differently [24–26], leading to a distribution of relaxation times and the appearance of stretched exponentials [27].

Field-dependent T_1 measurements were performed at two temperatures, 1.55 K and 4.6 K (Fig. 12), in the short-range-correlated phase as determined from previous heat capacity data [18] and above magnetic transitions ($T_N \sim 0.7$ K). At 1.55 K there is a peak in the relaxation rate ($1/T_1$) around 6 T, where the macroscopic magnetization reaches 20% of its saturation value which disappears upon heating the system at 4.6 K closer to the paramagnetic state. This might be the finite-temperature signature of the boundary between VC and SDW_2 phases which was theoretically predicted at 20% of the saturated magnetization M_s [8,28]. At still higher fields, a quadrupolar nematic phase is expected above 70% of M_s. The magnetization curve in that field region is very steep, and the field interval in which one may expect a QN phase is very narrow. The exact field value of the phase boundary between SDW_2 and QN is still unspecified; however a qualitative change of the temperature dependence of $1/T_1$ should definitely mark this boundary. More specifically, from theory in strictly 1D systems with a magnetic transition only allowed at $T = 0$ K, $1/T_1$ at very low temperatures should follow a power-law behavior $1/T_1 \propto T^{2\kappa-1}$ in both SDW_2 and QN phases, with $\kappa \in [0,1]$ being a field-dependent Tomonaga-Luttinger parameter [9,29]. The boundary between the two phases occurs at a field where $\kappa = 1/2$, roughly when 70% of saturation magnetization is reached. In the SDW_2 phase ($\kappa < 1/2$) one therefore expects a power-law divergence of $1/T_1$ at low temperatures, while for the QN phase ($\kappa > 1/2$) a power-law drop towards zero is predicted.

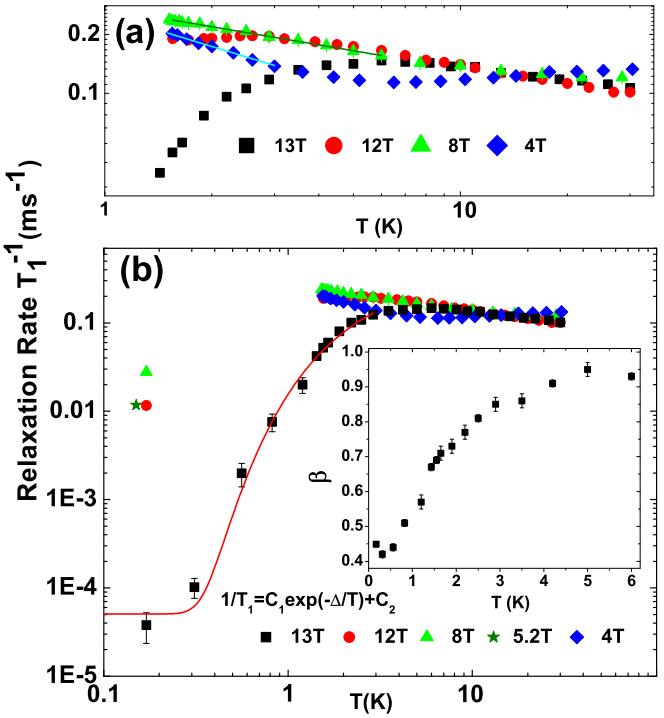

FIG. 13. (a) Temperature dependence of the spin lattice relaxation T_1^{-1} in magnetic fields $\mu_0 H = 4$, 8, and 12 T. At 4 T and 8 T the relaxation rate obeys power-law behavior down to 1.55 K with critical exponents $-0.55(2)$ and $-0.27(1)$, respectively. At 12 T and 13 T broad maxima appear, but the drop at 13 T below 2.2 K is too steep to be assigned to a QN phase. (b) Additional low-temperature (DR) measurements down to 125 mK. 13 T data below 2.9 K were fitted to the function $1/T_1 = C_1 \exp(-\Delta/T) + C_2$, where $\Delta = 3.24(19)$ K, with $C_1 = 0.396(47)$ m s^{-1} and $C_2 = 5.1(1.4) \times 10^{-5}$ m s^{-1}. Inset: T dependence of the stretched exponent β, indicating a broad distribution of relaxation times at low temperatures.

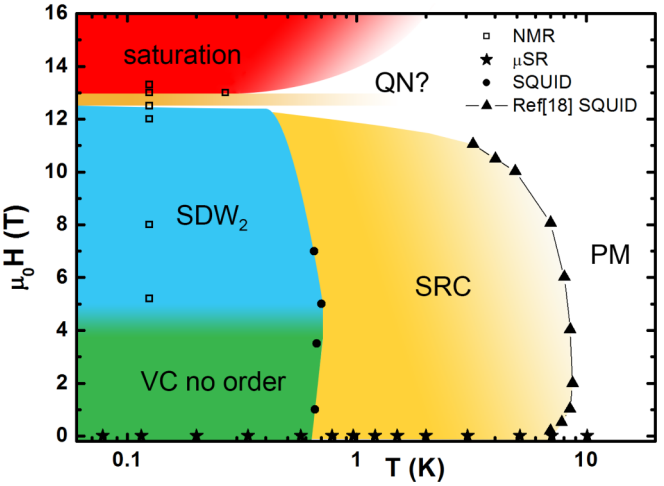

FIG. 14. Low-temperature phase diagram of $LiCuSbO_4$. Above 9 K, the system is in the paramagnetic regime (PM, white). As the temperature is lowered short-range correlations (SRC) among neighboring spins appear (yellow). However, from the width of NMR spectra in the temperatures down to 1.5 K at various fields (4 T, 8 T, 12 T, 13 T), one can clearly dismiss any kind of 3D order (this point was omitted from the phase diagram for clarity). Below 0.7 K, the system enters in a vector chiral (VC) regime with no static order in the fields up to ≈4 T. Above 4 T a crossover to an ordered SDW_2 phase occurs, as evidenced by NMR (blue). At high field and low temperature there is a narrow possibility for the existence of the QN phase (orange), just below the saturation regime (red).

Above the saturation field, the system is gapped and $1/T_1$ should decay exponentially towards zero. With this in mind, we chose fields of $\mu_0 H_0 = 4,8,12$, and 13 T to follow the temperature dependence of the relaxation rate (Fig. 13).

In $\mu_0 H_0 = 4$ T, where the VC phase is expected, $1/T_1$ shows traces of divergence down to 1.55 K with a critical exponent $1/T_1 \propto T^{-0.55(2)}$ [$\kappa = 0.24(1)$]. In $\mu_0 H_0 = 8$ T, where the SDW_2 phase is expected, $1/T_1$ shows a similar behavior down to 1.55 K with a critical exponent $1/T_1 \propto T^{-0.30(1)}$ [$\kappa = 0.38(1)$]. The exact values of κ are sensitive to the range over which they are fitted, but it is clear that they monotonically increase with field, as theoretically expected. Macroscopic magnetization measurements indicate that $\mu_0 H_0 = 12$ T is close to the SDW_2/QN phase boundary. The temperature dependence of $1/T_1$ shows a broad maximum around 2.5 K which might indicate the proximity of the QN phase. In $\mu_0 H_0 = 13$ T a maximum in relaxation rate occurs at much higher temperature, around 6 K, but below 2.2 K, the drop is too steep to be credited to a QN phase. If we take into account DR measurements, the critical exponent is $1/T_1 \propto T^{3.6}$, which would give a nonphysical value of $\kappa = 2.3(1)$. A more likely explanation, consistent with the formerly discussed static measurements, is that the magnetization is already saturated at $\mu_0 H_0 = 13$ T, and the $1/T_1$ shows a gapped (exponential) behavior. The 13 T data below 2.9 K were then fitted to the function $1/T_1 = C_1 \exp(-\Delta/T) + C_2$, where $\Delta = 3.24(19)$ K, $C_1 = 0.396(47)$ m s^{-1}, and $C_2 = 5.1(1.4) \times 10^{-5}$ m s^{-1}. The latter T-independent relaxation likely accounts for the contribution of a tiny amount of impurities or defects. Hence, the temperature dependence of the spin-lattice relaxation time changes qualitatively and quantitatively in the narrow field range 12–13 T, from a power-law divergence characteristic of the SDW_2 phase to a gapped behavior characteristic for saturation range.

Finally, the relaxation rate measured at a single temperature point $T = 0.125$ K in the field $\mu_0 H_0 = 5.2$ T gave a significantly longer T_1 (86 ms) than at 1.55 K, showing that there exists a maximum in the relaxation rate somewhere in between these two temperatures. As already noted, a peak in the heat capacity is observed at 700 mK [18], which, together with an anomaly in the susceptibility measurements, may mark a phase transition causing the nonmonotonic behavior of the relaxation rates.

VII. DISCUSSION

In the following, we discuss the various low-temperature phases of $LiCuSbO_4$ in the light of known data from the present study and Ref. [18] and summarize our current understanding in the tentative phase diagram shown in Fig. 14. To label the various field-induced phases, we rely on the theoretical work by Sudan *et al.* [8]. From the latter study of frustrated spin chains, in $LiCuSbO_4$ with $J_1/J_2 = -2.22$, the magnetic

excitations of $p = 2$ bound spin flips should govern the phase diagram. Several field-induced ground states are predicted: (i) a vector chiral phase (VC) for $M/M_{sat} < 0.15$, (ii) an SDW_2 phase for $0.15 < M/M_{sat} < 0.7$, and (iii) a QN phase for $0.7 < M/M_{sat} < 1$. Using the NMR shift at 0.125 K from Fig. 10 as a measure of the magnetization, one estimates that $M/M_{sat} = 0.15$ occurs at $\mu_0 H \approx 5$ T, $M/M_{sat} = 0.7$ occurs at $\mu_0 H \approx 12$ T, and $M = M_{sat}$ occurs at $\mu_0 H \approx 13$ T.

Vector chiral phase. The main result obtained from μSR measurements is that in $LiCuSbO_4$ no 3D magnetic ordering occurs down to $T = 30$ mK in zero field, which is a comparative advantage to all known frustrated 1D chains. The possible reason lies in the crystal structure in which hard magnetization axes of adjacent chains are not parallel [18], thus preventing 3D ordering down to the lowest temperatures. This low-field low-temperature phase (labeled green in Fig. 14) is consistent with the theoretical prediction of the vector chiral (helical) magnetic ground state [8]. Here no static ordering can be stabilized by magnetic field and the dominant VC correlation functions are faster than the characteristic μSR (and NMR) time scale. Looking for the boundary between the VC phase and the predicted SDW_2 we notice that the susceptibility curves at 1 and 3.5 T (Fig. 4) show the same shape with a minimum close to 0.7 K while at higher fields the shape evolves suggesting a distinct magnetic phase. Additionally, the heat capacity curves shown in Fig. 3(b) of Ref. [18] are similar at 0 and 2 T and evolve gradually only above 4 T with the growing of a peak around $T = 0.7$ K. Therefore the boundary between the two phases seems to occur between 4 and 5 T. The gradual evolution of the heat capacity suggests rather a crossover than a sharp transition from the VC phase to the SDW_2 one.

SDW_2 *phase.* The NMR spectra measured at $T = 125$ mK at $\mu_0 H = 5.2$ and 8 T (Fig. 9) clearly show that magnetic ordering has occurred. This is confirmed by specific-heat measurements where a peak at $T = 0.7$ K clearly indicates a magnetic transition in this intermediate-field range. NMR relaxation measurements at $\mu_0 H = 8$ T above the transition temperature show the temperature dependence $1/T_1 \propto T^{-0.30(1)}$ consistent with a SDW_2 phase (negative exponent less than 1). These results give a strong indication that in the medium-field range between $\mu_0 H \approx 5$ and 12 T the theoretically predicted SDW_2 phase is indeed stabilized by the magnetic field.

Possible quadrupolar nematic phase. NMR relaxation measurements at $\mu_0 H = 12$ T show a negative slope above $T = 2.5$ K, consistent with the SDW_2 phase, but below $T = 2.5$ K the slope changes to positive which could be consistent with a QN phase (positive exponent less than 1). This behavior may point to the proximity of the crossover between SDW_2 and QN phases. Contrary to the SDW_2 phase, the QN phase should not broaden the NMR spectrum, which was recently pointed out by Orlova *et al.* [16] in $LiCuVO_4$ just below the saturation field. Inspection of Fig. 9 shows that the spectrum at $\mu_0 H = 12$ T is narrower than the spectra at $\mu_0 H = 5.2$ T and 8 T, but still broader than the spectra at higher fields. This again points to the proximity of the QN phase, yet still not reached. The spectrum at $\mu_0 H = 12.5$ T is still narrower, maybe consistent with the QN phase. From the line shift the magnetization $M/M_{sat} = 0.85$ is theoretically in the QN phase ($M/M_{sat} > 0.7$) but the QN phase could be pushed to even higher magnetization for systems with hard-axis anisotropy [28]. NMR relaxation measurements down to the lowest temperatures may help in deciding whether the QN phase is realized at this field. In any case the lower boundary of the QN phase should be close to 12.5 T. On the other hand at $\mu_0 H = 13$ T the full saturation is reached, giving the upper boundary for the possible QN phase.

Saturation regime. When the saturation is reached one expects a gap in the excitation spectrum. This is confirmed by our relaxation measurements in the dilution refrigerator shown in Fig. 13(b) which yield the gap value $\Delta \approx 3.2$ K at 13 T. A theoretical model for the isotropic case [7] predicts the opening of the gap (i.e., the entrance in the saturation regime) when the ratio of the spin magnetic energy $\epsilon_s = g\mu_B\mu_0 H_s$ and the NNN interaction J_2 reaches $\epsilon_s/J_2 \approx 0.5$ which is in excellent agreement with our case (for $g = 2.21$ [18] in a field of $\mu_0 H_0 = 13$ T, $\epsilon_s = 18.2$ K, while $J_2 = 34$ K).

Grafe *et al.* [19] recently reported extensive experimental and theoretical research on $LiCuSbO_4$. NMR measurements were performed up to 16T on an unoriented powder sample, in a temperature range down to 2 K, preventing them from investigating the $T \to 0$ K phase diagram. Nonetheless in the temperature and field range common to our study, the NMR results are consistent. In particular at 13 T they also observed a gapped behavior of T_1, with a gap value $\Delta \approx 2.4$ K which is similar to our value. The main discrepancy with the present study is the determination of the saturation field which is of great importance in order to put an upper boundary on the QN phase. In Ref. [19], the magnetization curve obtained from bulk measurement using pulsed fields at 0.45 K did not reach saturation up to the highest measured field of 20 T, which was interpreted as a signature of in-plane exchange anisotropy ($J_1^x \neq J_1^y$). On the contrary our NMR shift data point to a well-defined saturation field close to 13 T and do not demand modifications of the magnetic model.

For the other QN candidate, $LiCuVO_4$, where high-quality single crystals are available, the NMR spectra could be followed in detail and match the two criteria for a QN phase, shift variation, and minimal width [16]. The quality of the sample needed and the detailed information on the hyperfine tensors are available for this compound. Yet the absence of T_1 measurements due to the high saturation field remains a severe bottleneck to the definitive proof of a QN phase.

So far we have interpreted our results guided by the theory for isotropic J_1-J_2 chains while our compound possesses a small easy-plane anisotropy (≈0.8) [18]. A detailed analysis of phase diagram in such anisotropic case is given in Ref. [28]. Easy-plane anisotropy favors the vector chiral phase, but if the anisotropy is not considerably pronounced, the QN phase still may exist in the high-field regime. This is a possible reason why the QN phase is restricted to such a narrow field range just below the saturation. The presence of a small interchain coupling may further narrow down the QN stability domain [30].

VIII. SUMMARY

$LiCuSbO_4$ features a very rich phase diagram with the possibility of having an exotic, not yet observed QN phase.

In the limit $T \to 0$ the ground state depends heavily on the applied magnetic field. In zero field no 3D ordering is observed down to 30 mK, although μSR shows traces of short-range correlations. This low-field phase is identified with a theoretically predicted vector chiral phase. The crossover between the vector chiral and the higher field spin density wave SDW_2 phase occurs between 4 T and 5 T. Indeed, above this crossover, the broadening of the NMR spectra reveals an induced 3D magnetic ordering on the scale of 0.75 μ_B. Further, the field-dependent NMR shift data at 125 mK enable a precise determination of the saturation field, which turns out to occur sharply and close to 13 T.

The NMR spectrum is still broad at 12 T, contrary to the predictions for the QN phase. However, the spectrum at 12.5 T is narrower and featureless, while its shift indicates that the magnetization is not yet saturated. This is one signature of a QN phase, namely the absence of rotation symmetry breaking just below the saturation field. Hence, combined with the change of behavior of the T dependence of the relaxation rate, we point to the possible existence of a QN phase in a narrow field range between 12.5 T and 13 T.

Our study provides a strong motivation to refine the investigations in a still very accessible field range as compared to other J_1-J_2 candidates and look for the final signatures of the long-sought QN phase in spin chain systems. If the direct observation of the elusive order parameter of a QN phase is cumbersome, two theoretical predictions on experimental observables indeed pave the way: NMR relaxation measurements should be performed down to very low temperature following Refs. [9,29], as pointed out in Ref. [31], and ESR might reveal excitation of bound magnon pair typical of a QN phase [32].

ACKNOWLEDGMENTS

This work was supported by the Croatian Science Foundation (HRZZ), Grant No. IP-11-2013-2729, the French Agence Nationale de la Recherche under "SPINLIQ" Grant No.ANR-12-BS04-0021, the Université Paris-Sud under a "PMP" MRM grant, and the Région Ile-de-France under a "MAGMAT" SESAME grant. The authors thank Ivica Živković for complementary measurements and Jeffrey Quilliam for useful discussions.

APPENDIX A: ANGLE-DEPENDENT ORIENTED POWDER SPECTRA

After the hardening of the mixture of epoxy glue and the powder sample, the orientation was checked by measuring the angular dependence of the NMR spectra in the magnetic field of 3 T as shown in Fig. 15. The quadrupole satellites of the strongly coupled line are most pronounced when the magnetic field is applied in the direction of the hard axis, which means that the eigenvector corresponding to the electric field gradient tensor component V_{zz} points in the direction of the hard axis (within an experimental error of $\approx 10^\circ$). As soon as the applied field is not parallel to the hard axis, the powder spectra narrow down and the spectral analysis becomes cumbersome. The inset of Fig. 15 shows the unoriented vs oriented powder spectrum in the magnetic field of 7.5 T. In the unoriented powder spectrum (black line) the quadrupole satellites cannot be resolved. For consistency we made a couple of oriented powder samples which have shown identical spectra when the applied field was parallel to the hard axis.

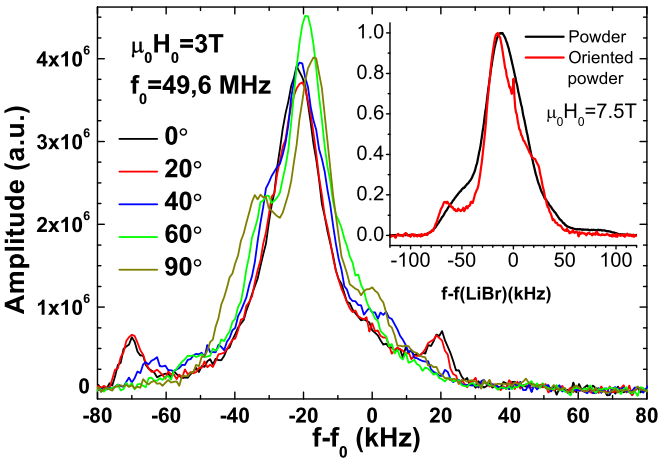

FIG. 15. Room temperature spectra at $\mu_0 H = 3$ T for different orientations of the applied field in the bc plane. The quadrupolar splitting is broadest when the applied field is parallel to the hard axis (0°). Inset: Unoriented vs oriented powder spectrum measured at $\mu_0 H = 7.5$ T. The small peak at zero shift comes from the LiBr reference signal.

APPENDIX B: RELAXATION FIT PARAMETERS

As mentioned in Sec. VI, at the peak position the spectra have contributions from both the strongly and weakly coupled lines, with different relaxation times. To determine the contribution of the weakly coupled line which corresponds to the function $f(\tau_1)$ in Eq. (4) we measured the relaxation on the right side of the spectra at 30% of the peak value where the contribution of the strongly coupled site is negligible. The relaxation curves of the weakly coupled line reveal two different relaxation regimes: a fast one with a relaxation time T_{1b} shorter than T_1 of the strongly coupled site, but of the same order of magnitude, and a long one T_{1c} which is several orders of magnitude longer than T_1 and T_{1b} at low temperatures. Our main goal was to fix T_{1b} so we could isolate T_1 in Eq. (4). We used the function $f(\tau_1)$ (for the weakly coupled site):

$$f(\tau_1) = be^{-(\tau_1/T_{1b})^{\beta_b}} + ce^{-(\tau_1/T_{1c})^{\beta_c}}. \quad \text{(B1)}$$

Having set $(1 - a) = 0.28$ in Eq. (4), the weights $b = \frac{0.22}{0.28}$ and $c = \frac{0.06}{0.28}$ were determined to fit the contributions of the fast and slow relaxation processes. The stretch parameters β_b and β_c were fixed to 1 above 1.55 K and left as free parameters at lower temperature measurements.

Spectra taken in $\mu_0 H_0 = 12$ T at different temperatures show indeed that the spectral shape does not change appreciably between 1.55 K and 30 K, and we take the coefficients a, b, and c as temperature independent. The spectral shape does not change either between 12 T and 13 T at 1.55 K, and we conclude that these parameters are field independent as well (for high fields). The parameter M_∞ was taken from the last measured point at $\tau_1 > 7 \times T_1(T_{1b})$, limited by the repetition time which had to be reasonably short in order to

make measurements possible. The total signal did not relax completely between two acquisitions, but this affects only the value of the longest relaxation time T_{1c}. Since T_{1c} is an order of magnitude longer than T_1 and T_{1b}, it turns out that its exact values are not critical for the determination of T_1. The values of T_{1b} were determined for each temperature and fixed before the T_1 in Eq. (4) was calculated. The stretch parameter β_b ranges from 0.51 at lowest temperature to 1 at 1.55 K.

[1] K. Penc and A. M. Läuchli, in *Introduction to Frustrated Magnetism*, edited by P. Mendels, C. Lacroix, and F. Mila (Springer, Heidelberg, 2011).

[2] M. Blume and Y. Y. Hsieh, J. Appl. Phys **40**, 1249 (1969).

[3] A. Andreev and I. Grishchuk, Zh. Eksp. Teor. Fiz. **87**, 467 (1984) [JETP **60**, 267 (1984)].

[4] F. Heidrich-Meisner, A. Honecker, and T. Vekua, Phys. Rev. B **74**, 020403 (2006).

[5] T. Vekua, A. Honecker, H.-J. Mikeska, and F. Heidrich-Meisner, Phys. Rev. B **76**, 174420 (2007).

[6] M. Sato, T. Hikihara, and T. Momoi, Phys. Rev. Lett. **110**, 077206 (2013).

[7] L. Kecke, T. Momoi, and A. Furusaki, Phys. Rev. B **76**, 060407 (2007).

[8] J. Sudan, A. Lüscher, and A. M. Läuchli, Phys. Rev. B **80**, 140402 (2009).

[9] M. Sato, T. Momoi, and A. Furusaki, Phys. Rev. B **79**, 060406 (2009).

[10] A. A. Gippius, E. N. Morozova, A. S. Moskvin, A. V. Zalessky, A. A. Bush, M. Baenitz, H. Rosner, and S.-L. Drechsler, Phys. Rev. B **70**, 020406 (2004).

[11] S. Giri, H. Chudo, H. Nakamura, and M. Shiga, J. Alloys Compd. **326**, 61 (2001).

[12] Y. Hoshino, S. Atarashi, T. Goto, M. Hase, and T. Sasaki, JPS Conf. Proc. **3**, 014012 (2014).

[13] M. Hase, H. Kuroe, K. Ozawa, O. Suzuki, H. Kitazawa, G. Kido, and T. Sekine, Phys. Rev. B **70**, 104426 (2004).

[14] M. Enderle, C. C. Mukherjee, B. Fak, R. K. Kremer, J.-M. Broto, H. Rosner, J. Richter, S.-L. Dreschler, J. Richter, J. Malek, A. Prokofiev, W. Assmus, S. Pujol, J.-L. Raggazzoni, H. Rakoto, M. Rheinstadter, and H. M. Ronnow, Europhys. Lett. **70**, 237 (2005).

[15] B. Willenberg, M. Schäpers, K. C. Rule, S. Süllow, M. Reehuis, H. Ryll, B. Klemke, K. Kiefer, W. Schottenhamel, B. Büchner, B. Ouladdiaf, M. Uhlarz, R. Beyer, J. Wosnitza, and A. U. B. Wolter, Phys. Rev. Lett. **108**, 117202 (2012).

[16] A. Orlova, E. L. Green, J. M. Law, D. I. Gorbunov, G. Chanda, S. Krämer, M. Horvatić, R. K. Kremer, J. Wosnitza, and G. L. J. A. Rikken, Phys. Rev. Lett. **118**, 247201 (2017).

[17] E. Cemal, M. Enderle, R. K. Kremer, B. Fak, E. Ressouche, M. V. Gvozdikova, M. E. Zhitomirsky, and T. Ziman, arXiv:1707.08051.

[18] S. E. Dutton, M. Kumar, M. Mourigal, Z. G. Soos, J.-J. Wen, C. L. Broholm, N. H. Andersen, Q. Huang, M. Zbiri, R. Toft-Petersen, and R. J. Cava, Phys. Rev. Lett. **108**, 187206 (2012).

[19] H.-J. Grafe, S. Nishimoto, M. Iakovleva, E. Vavilova, L. Spillecke, A. Alfonsov, M.-I. Sturza, S. Wurmehl, H. Nojiri, H. Rosner, J. Richter, U. K. Rößler, S.-L. Drechsler, V. Kataev, and B. Büchner, Sci. Rep. **7**, 6720 (2017).

[20] K. Momma and F. Izumi, J. Appl. Crystallogr. **44**, 1272 (2011).

[21] S. J. Blundell, Contemp. Phys. **40**, 175 (1999).

[22] A. Yaouanac and P. Dalmas de Réotier, *Muon Spin Rotation, Relaxation, and Resonance* (Oxford University Press, Oxford, UK, 2011).

[23] Y. J. Uemura, in *Muon Science*, edited by R. Cywinski, S. Kilcoyne, and S. Lee (Scottish Universities Summer School in Physics & IoP Publishing, Bristol, Philadelphia, 1998).

[24] S. Eggert, O. F. Syljuåsen, F. Anfuso, and M. Andres, Phys. Rev. Lett. **99**, 097204 (2007).

[25] S. Shinkevich, O. F. Syljuåsen, and S. Eggert, Phys. Rev. B **83**, 054423 (2011).

[26] F. Tedoldi, R. Santachiara, and M. Horvatić, Phys. Rev. Lett. **83**, 412 (1999).

[27] T. Shiroka, F. Casola, V. Glazkov, A. Zheludev, K. Prša, H.-R. Ott, and J. Mesot, Phys. Rev. Lett. **106**, 137202 (2011).

[28] F. Heidrich-Meisner, I. P. McCulloch, and A. K. Kolezhuk, Phys. Rev. B **80**, 144417 (2009).

[29] M. Sato, T. Hikihara, and T. Momoi, Phys. Rev. B **83**, 064405 (2011).

[30] O. A. Starykh and L. Balents, Phys. Rev. B **89**, 104407 (2014).

[31] F. Mila, Physics **10**, 64 (2017).

[32] S. C. Furuya and T. Momoi, arXiv:1707.08784.